The Hyperfine Structure of Potassium-40

Lindsay J. LeBlanc

April 12, 2006

1 Introduction

In the world of atomic physics, the alkali atoms sit in a place of honour. The basis for their continued popularity is their relatively simple structure - they look a lot like hydrogen, Nature's simplest atom. In this seat, they have become the tool physicists use to test their theories of a number of physical phenomena. The realisation of Bose-Einstein Condensation (BEC) in a dilute gas of alkali atoms (Na, Li) in 1995 [1] after years of futile attempts to do the same with hydrogen made the alkalis an ever more useful tool.

Dilute gases of neutral alkali atoms have been used to cleanly demonstrate a number of fascinating physical effects, including interference of matter waves [2], the transition to the Mott-insulator phase [3] and other superfluid effects such as the creation of vortices [4]. Most work done in so-called "cold atom" experiments has been done with bosonic species, since most of the alkali isotopes are bosons, and since the last step towards quantum degeneracy relies on collisions between cold atoms (for evaporative cooling [5]), which are forbidden between cold fermions. However, these obstacles have been overcome by cooling non-identical particles simultaneously and allowing for collisions between species to perform the evaporative cooling. The first realisation of Fermi degeneracy was in 1999, and has been followed by a number of other experiments [6].

Experiments with ultra-cold fermions are especially exciting in that they allow for the physics of condensed matter systems to be explored within the realm of atomic physics. The behaviour of fermionic atoms is analogous to that of the fermionic electrons that establish the physics of condensed matter. The precise control and measurement afforded by atomic systems is in stark contrast to condensed matter systems, where the structure of a sample is fixed and where impurities will always exist. Dilute atomic gases can be manipulated in many ways; the interactions between particles can be changed, the potentials in which they sit are easily controlled, and their distributions in momentum- or position-space are readily found.

Unlike bosons, there are only two stable alkali isotopes which are fermionic - ^{6}Li and ^{40}K. The choice between the two generally depends on the scattering properties needed for a particular experiment. Potassium atoms have a repulsive interaction at low temperatures, while Li atoms are attracted to one

another. This report will focus on ^{40}K, which is used in a number of laboratories throughout the world.

Knowledge of the structure of ^{40}K is crucial when performing experiments using this atom. To address specific states of the atom, the hyperfine structure should be well-understood. This report endeavours to calculate the hyperfine splitting in the ^{40}K atom, as a function of magnetic field (taking into account the Zeeman effect), and to calculate the transition matrix elements, which will give the probabilities for transitions between different hyperfine states under the influence of an optical field. Props to Daniel Steck for inspiring this compilation; his collection of ^{87}Rb data [7] is incredibly useful, and this is an attempt to begin the same for ^{40}K.

2   Fine Structure

A quick glance at the periodic table reveals that the alkali atoms (Li, Na, K, Rb, Cs, Fr) fall beneath hydrogen, that one atom for which wavefunctions are calculated in beginning quantum mechanics courses. To good approximation, the alkalis are considered "hydrogen-like" in that they have a single electron in the s-state orbitting a charged core, which for hydrogen is just the nucleus, and for the higher atomic numbers is the nucleus surrounded by closed shell electron orbitals. The Coulomb interaction of this electron with the core, together with the interaction between the angular momenta of the electron's orbit and its spin, gives rise to the discretisation of energy levels for the electron, known as the fine structure.

For an electron orbitting a charged core, we consider an angular momentum, **L**, associated with the orbital angular momentum, and an intrinsic angular momentum, **S**, which is the spin of the electron. These are coupled through the *spin-orbit* interaction [8] and we are free to label these energy levels by the value of the total angular momentum of the electron, **J**.

In that which follows, the two fine structure transitions that will be considered are the two lowest lying transitions. Since, by selection rules, L must change by one in a transition, the first two transitions from the ground state ($L = 0$) are to the $L = 1$ state. These two lines are known as the D1 and the D2 lines, for angular momentum $J = \frac{1}{2}$ and $J = \frac{3}{2}$ respectively, where $\mathbf{J} = \mathbf{L} + \mathbf{S}$ and J follows the triangle rule (i.e., $|L - S| \leq J \leq L + S$).

Given that the fine structure splitting is most accurately determined by experiment, measured values will be used. Table 1 gives the fine structure splitting for the D1 and D2 lines of ^{40}K in units of the wavelength of light which drives the transitions between them.

3   Hyperfine Structure

The next degree of precision in determining the energy levels of the alkali atom is to consider the effect of the nucleus. There will be two main contributions to

Atomic number (Z)	19	
Total nucleons ($Z + N$)	40	
Relative natural abundance	0.0117%	[9]
Atomic mass (m)	39.963886(28) amu	[9]
Nuclear spin (I)	4	[9]
D1 Transition Wavelength (^{2}S$_{1/2} \rightarrow {}^2$P$_{1/2}$)	770.10929 nm	[10]
D2 Transition Wavelength (^{2}S$_{1/2} \rightarrow {}^2$P$_{3/2}$)	766.70207 nm	[10]

Table 1: General properties of ^{40}K

the Hamiltonian which describes the energy of the atom: one due to the effective magnetic field arising from the spin of the nucleus, **I**, the other from the finite extent of the charge distribution of the nucleus and the associated higher order electric multipole moments.

3.1 Effects of nuclear spin

In the first approximation, nuclear spin is neglected because of the large mass of the nucleus in comparison to the electron. In going beyond the fine structure calculations, it is, however, one of the first things for which we must account. In simple terms, the spin of the nucleus interacts with the effective magnetic field created by the orbital electron or with an external magnetic field.

3.1.1 Internal effects

As with the electron spin, **S**, we can associate with the nucleus an intrinsic angular momentum, or spin, which shall be called **I**. It is the result of the addition of the spins of each of the constituent particles in the nucleus, and is determined by experiment. The spin of the ^{40}K nucleus is $I = 4$ [9]. [As a note of interest, it is the spin of the nucleus which determines whether the atom is a boson or fermion. Since half-integer spin particles are fermions, and the spin of the single valence electron is always $S = {}^1/_2$, fermionic alkalis have integer spin nuclei, which means they must have an even number of particles (since protons and neutrons also have $S = {}^1/_2$). Therefore, the mass number of a fermionic alkali is even (like ^{40}K) while bosons have odd mass numbers (like ^{87}Rb).]

In the absence of an external magnetic field, we can write a term in the Hamiltonian that accounts for the magnetic field of the electron,

$$H_{\text{B,el}} = -\frac{\boldsymbol{\mu}_I}{\hbar} \cdot \mathbf{B_J} \tag{1}$$

where $\boldsymbol{\mu}_I$ is the magnetic moment of the nucleus, $\mathbf{B_J}$ is the effective magnetic field due to the orbiting electron, defined by its angular momentum, **J**. Whereas with the fine structure, we considered LS coupling, here, we consider IJ coupling, that is, we consider that there are separate electron energy levels well defined by the angular momentum **J**, which are much smaller than the energy

levels calculated in the fine structure. A result of this approximation is that I and J will be two good quantum numbers. Using this, we can take the nuclear magnetic moment to be proportional to its angular momentum and apply the projection theorem [8]

$$\mu_I = \frac{\boldsymbol{\mu}_I \cdot \mathbf{I}}{I(I+1)} \mathbf{I} = g_I \mu_N \mathbf{I} \tag{2}$$

where we define an effective g-factor for the nucleus, g_I and make use of the nuclear magneton, $\mu_N = m_e/m_N \cdot \mu_B$, which is related to the Bohr magneton, μ_B. This expression is written, for clarity, as

$$\boldsymbol{\mu}_I = \frac{\mu_I}{I} \mathbf{I}. \tag{3}$$

Since, in writing down Eq. (1) we assume that B_J acts only in the electronic (and not the nuclear) subspace, we can assume it is proportional to $\mathbf{J}$ and we obtain an expression

$$H_{\mathrm{B,el}} = A_{\mathrm{hfs}} \mathbf{I} \cdot \mathbf{J} \tag{4}$$

where A is some yet-to-be-defined parameter, which is also measured experimentally. To find an expression for A, we must consider the magnetic field at the nucleus due to the orbital motion of the electron and the spin magnetism of the electron some distance from the nucleus. Such an expression can be obtained by considering the magnetic dipole moment in classical electromagnetism, and the expression for the Hamiltonian is given by Ref. [11]:

$$B_{el} = \frac{\mu_0}{4\pi} \left\{ -\frac{8\pi}{3} \boldsymbol{\mu}_e \delta(\boldsymbol{r}) + \frac{1}{r^3} \left[\boldsymbol{\mu}_e \cdot \boldsymbol{\mu}_N - 3\frac{(\boldsymbol{r} \cdot \boldsymbol{\mu}_e)\boldsymbol{r}}{r^2} - \frac{e}{m}\boldsymbol{L} \right] \right\}. \tag{5}$$

where $\boldsymbol{\mu}_e = -2\mu_B \mathbf{S}$ with $g_s = 2$. Inspection of this term reveals that the first term vanishes for all states with $L \geq 1$, since these wavefunctions vanish at the origin. For these states,

$$H_{\mathrm{B,el}} = \left(\frac{2\mu_0 \mu_B \mu_I}{4\hbar\pi I} \right) \frac{\mathbf{I} \cdot \mathbf{N}}{r^3} \tag{6}$$

with

$$\mathbf{N} = \mathbf{L} - \mathbf{S} + \frac{3(\mathbf{S} \cdot \mathbf{r})\mathbf{r}}{r^2}. \tag{7}$$

Since we wish to consider states diagonal in $\mathbf{J}$, we may use the projection theorem, recognising that the operator $\mathbf{N}$ is a vector operator (it has components like $\mathbf{r}$), and obtain an expression [12]

$$H_{\mathrm{B,el}} = \left(\frac{2\mu_0 \mu_B \mu_I}{4\hbar\pi I} \right) \frac{\mathbf{N} \cdot \mathbf{J}}{J(J+1)} \frac{\mathbf{I} \cdot \mathbf{J}}{r^3}. \tag{8}$$

The term $\mathbf{N} \cdot \mathbf{J}$ can be rewritten using $\mathbf{J} = \mathbf{L} + \mathbf{S}$ as

$$\mathbf{N} \cdot \mathbf{J} = \mathbf{L}^2 - \mathbf{S}^2 + 3(\mathbf{S} \cdot \mathbf{r})(\mathbf{r} \cdot \mathbf{L})/r^2 + 3(\mathbf{S} \cdot \mathbf{r})(\mathbf{r} \cdot \mathbf{S})/r^2. \tag{9}$$

The third term vanishes since $\mathbf{r} \cdot \mathbf{L} = 0$ and the second and fourth terms also combine to give zero, which can be shown by writing out these terms in x, y, z components. This leaves $\mathbf{N} \cdot \mathbf{J} = \mathbf{L}^2$, such that within the fine structure manifold, this term remains constant, and we may write an expression for A_{hfs} in Eq. (4),

$$A_{\mathrm{hfs}} = \left(\frac{2\mu_0\mu_B\mu_I}{4\hbar\pi I}\right) \left\langle \frac{1}{r^3} \right\rangle \frac{L(L+1)}{J(J+1)}; \qquad L \neq 0. \tag{10}$$

For $L = 0$, Eq. (10) vanishes, but we are left with the first term from Eq. (4). Since $\mathbf{J} = \mathbf{S}$, we can write the Hamiltonian in a form like Eq. (4) and find an expression for $A(J)$

$$A_{\mathrm{hfs}} = \left(\frac{2\mu_0\mu_B\mu_I}{4\hbar\pi I}\right) \left(\frac{8\pi}{3}\right) |\psi(0)|^2; \qquad L = 0. \tag{11}$$

The parameter A_{hfs} is generally determined experimentally to greater precision than these approximations allow, and as such, the experimental parameters will be used in the calculations which follow.

3.1.2 External effects

In addition to the effects within the atom, the nuclear and electronic spins can also interact with external magnetic fields, which is commonly known as the Zeeman effect. The term in the Hamiltonian arising from the external magnetic field looks like

$$H_{\mathrm{B,ext}} = \frac{1}{\hbar}\left(\boldsymbol{\mu}_J \cdot \mathbf{B} + \boldsymbol{\mu}_I \cdot \mathbf{B}\right) \tag{12}$$

where the terms $\boldsymbol{\mu}_J = g_J\mu_B\mathbf{J}$ and $\boldsymbol{\mu}_I = g_J\mu_B\mathbf{I}$ define the g-factors. By invoking the projection theorem, expressions for the g_J factors can be obtained:

$$g_J = g_L\frac{J(J+1) - S(S+1) + L(L+1)}{2J(J+1)} + g_S\frac{J(J+1) + S(S+1) - L(L+1)}{2J(J+1)} \tag{13}$$

where g_L and g_S are experimentally determined values (the Landé g-factors) for the magnetic dipole moments of the electron spin and electron orbital, quoted in Table 2, along with the measured values of g_J, where available.

Expressions for the strong and the weak field limits of H_B are common in quantum mechanics or atomic physics textbooks (see, e.g. [13]). In the weak field, the $|F, m_F\rangle$ states are the eigenstates of the system and the total spin of the system must be taken into account, and the external field Hamiltonian can be written

$$H_{\mathrm{B,ext_{weak}}} = \frac{\mu_B}{\hbar}g_F\mathbf{F} \cdot \mathbf{B}. \tag{14}$$

where

$$g_F = g_J\frac{F(F+1) - I(I+1) + J(J+1)}{2F(F+1)} + g_I\frac{F(F+1) + I(I+1) - J(J+1)}{2F(F+1)}. \tag{15}$$

Similarly, an expression for the high field value of the magnetic field has eigenstates $|J, m_J, I, m_I\rangle$, where the effects on the orbital electron are far greater than those on the nucleus and the coupling is not important, the Hamiltonian becomes

$$H_{B,\text{ext}_{\text{strong}}} = \frac{\mu_B}{\hbar} \left(g_J \mathbf{J} + g_I \mathbf{I}\right) \cdot \mathbf{B}. \tag{16}$$

Here, I will be considering all magnetic fields and will use the $|J, m_J, I, m_I\rangle$ states to calculate the energy of the hyperfine interactions. Taking into account all effects due to the nuclear spin, we find a Hamiltonian

$$H_B = A_{\text{hfs}} \mathbf{I} \cdot \mathbf{J} + \frac{\mu_B}{\hbar} \left(g_J \mathbf{J} + g_I \mathbf{I}\right) \cdot \mathbf{B} \tag{17}$$

3.2   The electric quadrupole moment

In solving for the energy levels of a many-electron atom, one begins by using the approximation that the electrostatic interaction of the nucleus and the electron is that between two point charges. This amounts to considering only the monopole moment of the complete multipole expansion of the interaction. Results of such calculations will suffice to yield the fine structure of the atom. To go beyond this, the finite size of the nucleus must be accounted for, and can be done by considering an electric Hamiltonian of the form [14]

$$H_E = \frac{1}{4\pi\epsilon_0} \int_{\tau_e} \int_{\tau_n} \frac{\rho_e \rho_n d\tau_e d\tau_n}{|r_e - r_n|} \tag{18}$$

where $\rho_{e(n)}$ represents the charge distribution of the electron (nucleus) and $d\tau$ the volume elements for each. By assuming that $r_e > r_n$, we find that an expansion in terms of spherical harmonics can be made, and

$$H_E = \frac{1}{4\pi\epsilon_0} \sum_k \int_{\tau_e} \int_{\tau_n} \frac{\rho_e \rho_n}{r_e} \left(\frac{r_n}{r_e}\right)^k P_k(\theta_{en}) d\tau_e d\tau_n, \tag{19}$$

where θ_{en} is the angle subtended by r_e and r_n and

$$P_k(cos\theta_{en}) = \frac{4\pi}{2k+1} \sum_{q=-k} k(-1)^q Y_k^{(-q)}(\theta_n, \phi_n) Y_k^{(q)}(\theta_e, \phi_e) \tag{20}$$

where the $Y_k^{(q)}$ are the spherical harmonics.

This form of the expression is useful, for we may separate the dependence on nuclear and electronic coordinates such that

$$H_E^{(k)} = \mathbf{Q}^{(k)} \cdot (\nabla \mathbf{E}^e)^{(k)} = \sum_{q=-k}^{q} (-1)^q Q^{(q)} (\nabla E^e)_q^{(k)} \tag{21}$$

where

$$Q_q^{(k)} = \left(\frac{4\pi}{2k+1}\right)^{1/2} \int_{\tau_n} \rho_n r_n^k Y_k^{(-q)}(\theta_n, \phi_n) d\tau_n \tag{22}$$

and

$$(\nabla E^e)_q^{(k)} = \frac{1}{4\pi\epsilon_0} \left(\frac{4\pi}{2k+1}\right)^{1/2} \int_{\tau_e} \rho_e r_e^{-(k+1)} Y_k^q(\theta_e, \phi_e) d\tau_e. \qquad (23)$$

The first $(k = 0)$ term in this expansion yields the monopole moment, which is exactly that which was taken into account to realise the fine structure. The second term, the dipole moment, vanishes due to parity considerations. The electric nuclear Hamiltonian must remain invariant under inversion of the spatial coordinates, which means that expectation values of moments with odd powers of r^k vanish. As such, it is the quadrupole moment in which we are interested as a first correction to the fine structure.

Retaining only the quadrupole term, $(k = 2)$, Eqs. (22) and (23) can be written in tensor form [15]

$$Q_{ij} = \int_{\tau_n} \rho_n(\mathbf{r}_n) \left(3\frac{x_{ni}x_{nj} + x_{nj}x_{ni}}{2} - \delta_{ij}r_n^2\right) d\tau_n \qquad (24)$$

$$(\nabla E^e)_{ij} = \frac{1}{4\pi\epsilon_0} \int_{\tau_e} \frac{\rho_n(\mathbf{r}_e)}{r_e^2} \left(3\frac{x_{ei}x_{ej} + x_{ej}x_{ei}}{2} - \delta_{ij}r_e^2\right) .d\tau_e \qquad (25)$$

These tensors, it should be noted, are symmetric, and have zero trace. Further, since these tensors are constructed from elements (i.e. position operators) whose commutation properties with $\mathbf{I}$ are all the same, it has been shown that the matrix elements $\langle I, m_I|Q_{if}|I', m_I'\rangle$ all have the same dependence on the magnetic quantum number m_I [15]. This dependence can be gathered into a single constant, and we can write the nuclear quadrupole tensor

$$Q_{ij} = C\left[3\frac{\mathbf{I}_i\mathbf{I}_j + \mathbf{I}_j\mathbf{I}_i}{2} - \delta ij\mathbf{I}^2\right] \qquad (26)$$

where, if we define a scalar quantity, $Q = \frac{2}{e}\langle II|Q_{33}|II\rangle$, we can find C through

$$\begin{aligned}
Q &= \frac{2}{e}\int_{\tau_n} \rho_n[3z_n^2 - r_n^2]d\tau_n \\
&= \frac{2}{e}C\langle II|3\mathbf{I}_z^2 - \mathbf{I}^2|II\rangle \\
&= \frac{2}{e}C(3I^2 - I(I+1)) = \frac{2}{e}CI(2I-1) \qquad (27)
\end{aligned}$$

and obtain an expression

$$Q_{ij} = \frac{eQ}{2I(2I-1)}\left[3\frac{\mathbf{I}_i\mathbf{I}_j + \mathbf{I}_j\mathbf{I}_i}{2} - \delta ijI^2\right]. \qquad (28)$$

A similar procedure for the electric quadrupole tensor yields matrix elements diagonal in $\mathbf{J}$ to give

$$(\nabla E^e)_{ij} = \frac{-eq_J}{J(2J-1)}\left[3\frac{\mathbf{J}_i\mathbf{J}_j + \mathbf{J}_j\mathbf{J}_i}{2} - \delta ijJ^2\right]. \qquad (29)$$

7

	ground (^{2}S$_{1/2}$)	D1 (^{2}P$_{1/2}$)	D2 (^{2}P$_{3/2}$)
A_{hfs} (MHz)	-285.731(16) [16]	-34.49(11) [17]	-7.48(6) [17]
B_{hfs} (MHz)	n/a	n/a	-3.23(50) [17]
Isotope shift, $\Delta\nu$ (MHz) (relative to ^{39}K)	125.58(26) [17]	n/a	n/a
g_J	2.00229421(24) [18]	0.665885†	1.334102228†
g_I	0.000176490(34) [18]		
g_S	2.0023193043737(75) [19]		
g_L	0.99998627(25)* (from [19]		

Table 2: Electronic and magnetic parameters for ^{40}K. All values are determined experimentally unless otherwise noted. † Calculated using g_S, g_L with Eq. (13); * Calculated using $g_L = 1 - m_e/m_{nuc}$.

where

$$q_J = \frac{1}{e} \int_{\tau_e} \rho_{e,J} \frac{3z_e^2 - r_e^2}{r_e^5} d\tau_e \tag{30}$$

which gives a total electric quadrupole Hamiltonian $H_Q = Q_{ij}(\nabla E^e)_{ij}$.

Inspection of Eqs. (28) and (29) shows that since terms like $^3/_2(\mathbf{J_i J_j} + \mathbf{J_j J_i}) = 3\mathbf{J_z}$, the terms in square brackets vanish if $I = ^1/_2$ or $J = ^1/_2$. This is relevant to the structure of the alkalis in that the ground state and D1 hyperfine state energy shifts will have no contribution from the electric quadrupole term.

By combining terms through the use of commutation relations and performing some algebra [15], this gives

$$H_Q = \frac{e^2 q_J Q}{2I(2I-1)J(2J-1)} \left[3(\mathbf{I} \cdot \mathbf{J})^2 + \frac{3}{2}(\mathbf{I} \cdot \mathbf{J}) - \mathbf{I}^2 \mathbf{J}^2 \right]. \tag{31}$$

The coefficient $B_{\text{hfs} \equiv e^2 q_J Q}$ is generally used, and this has been measured for most elements, including ^{40}K (see Table 2).

4 Calculating the hyperfine splitting for all magnetic fields

Taking into account both the effects of the nuclear spin and the electric quadrupole moment (the latter only for the D2 line), the hyperfine Hamiltonian can be written,

$$H_{hfs} = A_{\text{hfs}}\mathbf{I} \cdot \mathbf{J} + B_{\text{hfs}} \frac{3(\mathbf{I} \cdot \mathbf{J})^2 + \frac{3}{2}\mathbf{I} \cdot \mathbf{J} - \mathbf{I}^2 \cdot \mathbf{J}^2}{2I(2I-1)J(J-1)} + \frac{\mu_B}{\hbar}(g_J m_J + g_I m_I)B \tag{32}$$

where all terms have been defined in §3. Experimental values for A_{hfs}, B_{hfs}, and the g-factors are given in Table 2.

The hyperfine splitting can be easily calculated in either the low magnetic field or the high magnetic field situations. In the first, the magnetic field dependent effects are treated as a perturbation and the good quantum numbers are given by $|F, m_F\rangle$. In the latter, the electric quadrupole term is treated perturbatively, and the states $|J, m_J, I, m_I\rangle$ define the good eigenstates. However, neither approach gives a complete description of the magnetic field dependence of the hyperfine splitting. To determine the energies at all values of the magnetic field, Eq. (32) must be numerically diagonalised.

To perform such a calculation, it is necessary to choose a set of states under which to write the original Hamiltonian. The $|J, m_J, I, m_I\rangle$ states are a good choice, as expressions for the matrix elements necessary for the calculation can be found. In particular, if we can determine the matrix elements with respect to the nuclear spin term of the Hamiltonian by considering the operator

$$\mathbf{I} \cdot \mathbf{J} = \mathbf{I}_z \mathbf{J}_z + \frac{1}{2}(\mathbf{I}_+ \mathbf{J}_- + \mathbf{I}_- \mathbf{J}_+) \tag{33}$$

using

$$\langle I, m_I \pm 1|I_\pm|I, m_I\rangle = \sqrt{(I \mp m_I)(I \pm m_I + 1} \tag{34}$$

and writing down the non-zero matrix elements for the operator (33) (See Appendix A).

Similarly, for the electric quadrupole term, it is useful to consider the operator

$$f = 3(\mathbf{I} \cdot \mathbf{J})^2 + \frac{3}{2}\mathbf{I} \cdot \mathbf{J} - \mathbf{I}^2 \cdot \mathbf{J}^2 \tag{35}$$

and determine the matrix elements with respect to it. These are also found in Appendix A.

Finally, the term involving the magnetic field is diagonal in the $|J, m_J, I, m_I\rangle$ basis, which makes the calculation of the relevant matrix elements relatively simple.

The actual calculation of the energies can be performed numerically, and was done using MATLAB. For each of the three manifolds considered, a vector containing each of the possible states was created, i.e. for the $^2S_{1/2}$ (ground) state, there are 18 substates defined all possible combinations of m_J and m_I where $-\frac{1}{2} \leq m_J \leq \frac{1}{2}$ and $-4 \leq m_I \leq 4$. The Hamiltonian matrix is constructed by calculating each element individually. For example, if the state vector is defined as (using an $|m_J, m_I\rangle$ notation)

$$\Psi_{m_J, m_I} = \begin{bmatrix} |^1/_2, 4\rangle \\ |^1/_2, 3\rangle \\ |^1/_2, 2\rangle \\ \vdots \end{bmatrix}$$
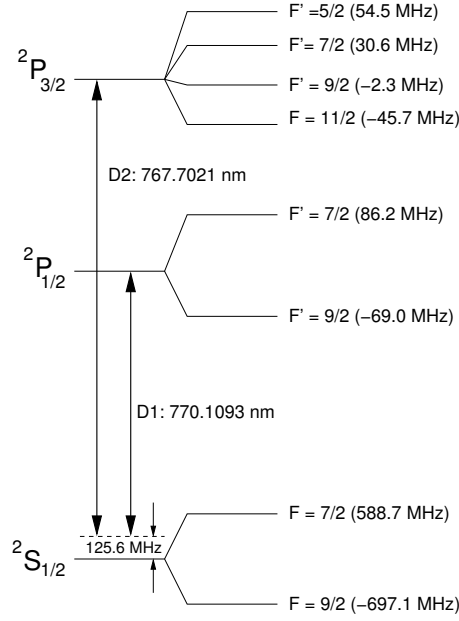
Figure 1: Level diagram for ^{40}K; calculated at zero magnetic field. All values derived from constants in Table 2.

then we may define an 18×18 Hamiltonian matrix as

$$
H_{\mathrm{hfs}} = \begin{bmatrix}
\langle ^1/_2, 4|H_{\mathrm{hfs}}|^1/_2, 4\rangle & \langle ^1/_2, 4|H_{\mathrm{hfs}}|^1/_2, 3\rangle & \langle ^1/_2, 4|H_{\mathrm{hfs}}|^1/_2, 2\rangle \cdots \\
\langle ^1/_2, 3|H_{\mathrm{hfs}}|^1/_2, 4\rangle & \langle ^1/_2, 3|H_{\mathrm{hfs}}|^1/_2, 3\rangle & \langle ^1/_2, 3|H_{\mathrm{hfs}}|^1/_2, 2\rangle \cdots \\
\langle ^1/_2, 2|H_{\mathrm{hfs}}|^1/_2, 4\rangle & \langle ^1/_2, 2|H_{\mathrm{hfs}}|^1/_2, 3\rangle & \langle ^1/_2, 2|H_{\mathrm{hfs}}|^1/_2, 2\rangle \cdots \\
\vdots & \vdots & \vdots & \ddots
\end{bmatrix} .
$$

This matrix is then calculated for a value of magnetic field, B, and numerically diagonalised. The energy eigenvalues are stored, and this process is repeated for 10 000 small increments in magnetic field. By plotting the energy eigenvalues for all magnetic field values, we find that the low field eigenstates gradually merge into the high-field eigenstates. A schematic of the zero-field structure is shown in Fig. (1). The results of the full calculations, shown in Figs. (2), (3), and (4) for the ground ($^2S_{1/2}$), D1 ($^2P_{1/2}$), and D2 ($^2P_{3/2}$) levels, demonstrate the gradual transformation from $|F, m_F\rangle$ states to the $|m_J, m_I\rangle$ states.

Another useful piece of information to emerge from these calculations is the set of eigenvectors valid for each magnetic field. MATLAB returns the eigenvector for each calculation, giving the coefficients of each element of (4) at each magnetic field value. These numerical values tell us how the $|m_J, m_I\rangle$ substates mix to form the real eigenstates. These values can be used to determine the overall transition rates at each value of the magnetic field (See §6).
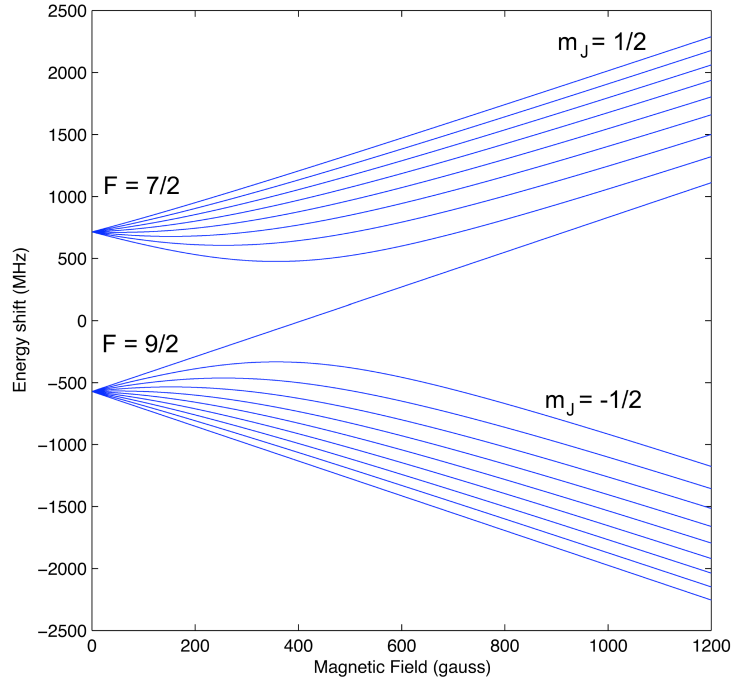
10

Figure 2: Hyperfine energy shift for the ground state (^{2}S$_{1/2}$) of ^{40}K as a function of magnetic field. The highlighted curve is used in the calculation in §.

5 Transition Matrix Elements

To manipulate and probe atoms in experiments, electromagnetic fields are used to couple energy levels to one another. In particular, levels with different J values are generally separated by energies corresponding to optical frequencies, allowing for the addressing of atoms with laser light.

When considering the interaction of atoms and electromagnetic fields, the electric dipole term is the largest perturbation to the atomic energy levels [20]. This operator, defined by

$$H_{E1} = -e\mathbf{r} \cdot \mathbf{E(0, t)} = \mathbf{d} \cdot \mathbf{E(0, t)} \tag{36}$$

where $E(0, t)$ is the time-dependent electric field at the origin, $\mathbf{r}$ is the position operator at the origin, and $\mathbf{d}$ is called the dipole operator, can be treated using time-dependent perturbation theory. Assuming that all transitions will be made with near-resonant light, the rotating wave approximation (RWA) is justified, and the radiative lifetime, and experimentally measurable quantity, can be expressed in terms of the dipole matrix elements, (see, for example, Ref. [21])

$$A_{if} = \frac{1}{\tau_{life}} = \frac{\omega_0^2 |\langle i|\mathbf{d}|f\rangle|^2}{3\pi\epsilon_0 \hbar c^3}, \tag{37}$$
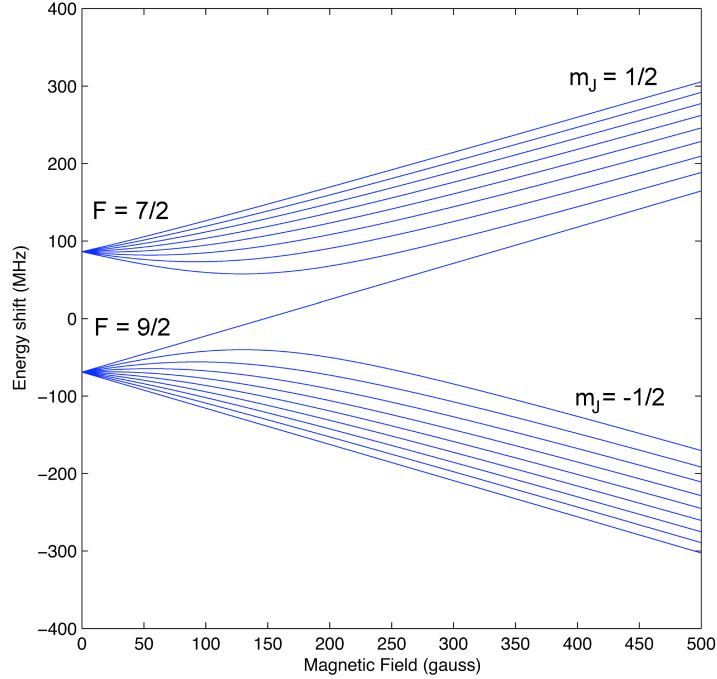
11

Figure 3: Hyperfine energy shift for the D1 manifold ($^2\mathrm{P}_{1/2}$) of $^{40}\mathrm{K}$ as a function of magnetic field

where τ_{life} is the radiative lifetime, ω_0 is the angular frequency of the electromagnetic field, i and f stand for the initial and final states, respectively, and A_{12} is the rate of decay between these states.

Expressing the position operator as a first-rank spherical tensor allows the application of the Wigner-Eckart theorem,

$$\mathbf{r} = \sum_{q=-1}^{1} T_q^{(1)} \mathbf{e}_q \tag{38}$$

where the $T_q^{(1)}$ are the first-rank spherical tensors, and the $\mathbf{e}_q$ are the unit direction vectors for each $T_q^{(1)}$. Each of these direction vectors represents a specific polarisation of the light field: $\mathbf{e}_{\pm 1}$ represent circularly polarised light ($\sigma^{\mp}$), while $\mathbf{e}_0$ is linearly polarised light (π-light, oriented parallel to the quantisation direction) and they form a complete basis for the polarisation. The Wigner-Eckart theorem is expressed as

$$\langle i|\mathbf{d}|f\rangle = e \sum_q \langle i||T^{(1)}||f\rangle \begin{pmatrix} P_i & 1 & P_f \\ -m_i & q & m_f \end{pmatrix} \mathbf{e}_q, \tag{39}$$

where we have introduced the reduced matrix element which is independent of m, q and a generalised angular momentum, P, which will be either J or F
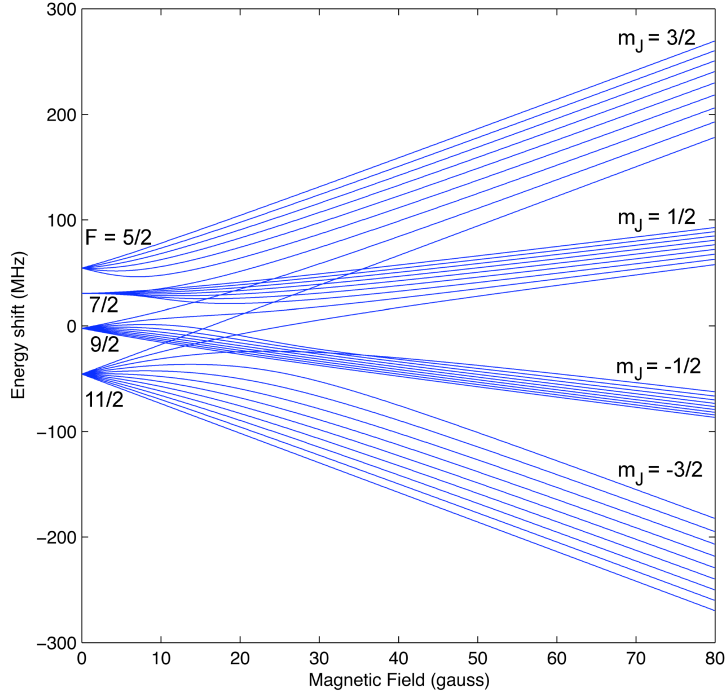
Figure 4: Hyperfine energy shift for the D2 manifold ($^2\mathrm{P}_{3/2}$) of $^{40}\mathrm{K}$ as a function of magnetic field. The highlighted curve is used in the calculation in §.

in that which is to follow. The term in brackets is the 3-j symbol and is a measure of the relative strength of transitions between initial and final states. The transition rate is then

$$A_{if} = \frac{\omega_0^3}{3\pi\epsilon_0 \hbar c^3} |\langle i||T^{(1)}||f\rangle|^2 \left\{ \sum_q \begin{pmatrix} P_i & 1 & P_f \\ -m_i & q & m_f \end{pmatrix}^2 \right\} \qquad (40)$$

where we have used the orthoganality of the $\mathbf{e}_q$ to give diagonal elements in q.

In general, we do not resolve the lifetime between states but instead consider a total decay from one excited level to the ground level. We may sum over all possible states within each level to obtain the result, and find that, using the normalisation condition for the 3-j symbols, the term under summation over q is simply $1/(2P_f + 1)$ [8].

With this in hand, we can express the reduced matrix element in terms of A_{if}^{tot} and the transition probability for each transition between states can be written using Eq. (39)

$$\langle i|\mathbf{d}|f\rangle = \left[\frac{3\pi\epsilon_0 \hbar c^3 (2P_f + 1) A_{if}^{tot}}{\omega_0^3} \right]^{1/2} \sum_q \begin{pmatrix} P_1 & 1 & P_f \\ -m_i & q & m_f \end{pmatrix} \mathbf{e}_q. \qquad (41)$$

13

	D1 (^{2}P$_{1/2}$)	D2 (^{2}P$_{3/2}$)	Ref.
τ_{life}^{tot} (ns)	26.79(7)	26.45(7)	[22]
$\langle J||\mathbf{d}||J'\rangle$ (C·m)	$3.478(5) \times 10^{-29}$	$4.917(7) \times 10^{-29}$	-

Table 3: Lifetimes of D1 and D2 levels and associated reduced matrix elements for ^{40}K.

We can give the term under the square root the designation $\langle i||\mathbf{d}||f\rangle$, a reduced matrix element for the dipole operator which, as it should be, is independent of q. Values for the radiative lifetime (that is, the time an atoms remains in the excited state before it decays back to the ground state) for the D1 and D2 excited states (defined by $P \rightarrow J$) have been measured and are given in Table 3, along with the associated $\langle J||\mathbf{d}||J'\rangle$.

5.1 High-field transition matrix elements

In strong magnetic fields, the states defined by quantum numbers $|J, m_J, I, m_I\rangle$ are good, as was seen in earlier discussion. The selection rules are $\Delta J = 0, \pm 1$, $\Delta L = \pm 1$, $\Delta m_J = 0, \pm 1$ and $\Delta m_I = 0$ [23]. We can see this by rewriting Eq. (39)

$$\langle J, m_J, I, m_I | d | J', m_J', I, m_I'\rangle = (-1)^{J'-1+m_J} \langle J||\mathbf{d}||J'\rangle \begin{pmatrix} J & 1 & J' \\ -m_J & q & m_J' \end{pmatrix} \langle I, m_I | I', m_I'\rangle, \tag{42}$$

where the final matrix element dictates the selection rule $m_I = m_I'$ (as the nuclear part is unaffected by the dipole field) and the 3-j coefficients give the m_J selection rule. In general, we are interested in the relative probabilities for transitions between states, since all other factors remain the same for transitions within a given manifold. As such, it suffices to calculate the 3-j symbols and to compare them.

5.2 Low-field transition matrix elements

In weak magnetic fields, the states defined by quantum numbers $|F, m_F\rangle$ are good. Rewriting Eq. (39) in this case yields

$$\langle F, m_F | d | F', m_F'\rangle = (-1)^{F'-1+m_F} \langle F||\mathbf{d}||F'\rangle \begin{pmatrix} F & 1 & F' \\ -m_F & q & m_F' \end{pmatrix}. \tag{43}$$

The selection rules in the low-field regime are $\Delta F = 0, \pm 1$, $\Delta L = \pm 1$, $\Delta M_F = 0, \pm 1$, and $F = 0 \rightarrow F' = 0$ transitions are not allowed [23]. Unlike the high-field case, we do not have direct access to the reduced matrix element from experimental measurements. To connect it to the values presented in Table 3, we must make use of the 6-j symbols [24]. Considering a system of two parts, which, when combined, create a total angular momentum, we can connect either of the reduced matrix elements for the two parts with that for the complete

14

system. In particular, we consider a total angular momentum $\mathbf{F}$ and the two subsystems with angular momenta $\mathbf{I}$ and $\mathbf{J}$. Since $\mathbf{F} = \mathbf{I} + \mathbf{J}$, we can write, using the Wigner-Eckart theorem in the $\mathbf{J}$ and $\mathbf{F}$ systems and the completeness relationships for the 3-j symbols,

$$\langle F'||\mathbf{d}||F\rangle = (-1)^{J_{max}+I_+F_{min}+1} \sqrt{(2F+1)(2F'+1)} \begin{Bmatrix} J' & J & 1 \\ F & F' & I \end{Bmatrix} \langle J'||\mathbf{d}||J\rangle$$

(44)

where the term in the curly brackets is the 6-j symbol, and the min, max subscripts stand for the minimum or maximum values for F or J among the primed and unprimed variables.

To determine the overall transition matrix element for the $|F, m_F\rangle$ states, we substitute Eq. (44) into Eq. (43) and by collecting all coefficients (including 3-j and 6-j symbols into one, can obtain an expression

$$\langle F, m_F||\mathbf{d}||F', m'_F\rangle = C_F(F, m_F, J, q)\langle J'||\mathbf{d}||J\rangle$$

(45)

where the coefficients, depending on total angular momentum, F, hyperfine substate, m_F, total orbital angular momentum, J, and the polarisation of the excitation, q. These coefficients were calculated with the help of Mathematica and are tabulated in Tables 4 through 7.

	m_F	$-7/2$	$-5/2$	$-3/2$	$-1/2$	$1/2$	$3/2$	$5/2$	$7/2$
σ^+	$F'=7/2$	$-\dfrac{\sqrt7}{9\sqrt3}$	$-\dfrac{2}{9}$	$-\dfrac{\sqrt5}{9}$	$-\dfrac{4}{9\sqrt3}$	$-\dfrac{\sqrt5}{9}$	$-\dfrac{2}{9}$	$-\dfrac{\sqrt7}{9\sqrt3}$	0
	$F'=9/2$	$\dfrac{\sqrt2}{9\sqrt3}$	$\dfrac{\sqrt2}{9}$	$-\dfrac{2}{9\sqrt3}$	$\dfrac{2\sqrt5}{9}$	$\dfrac{\sqrt{10}}{9}$	$\dfrac{\sqrt{14}}{9}$	$\dfrac{2\sqrt{14}}{9\sqrt3}$	$\dfrac{2\sqrt2}{3\sqrt3}$
π	$F'=7/2$	$\dfrac{7}{9\sqrt6}$	$\dfrac{5}{9\sqrt6}$	$\dfrac{1}{3\sqrt6}$	$\dfrac{1}{9\sqrt6}$	$-\dfrac{1}{9\sqrt6}$	$-\dfrac{1}{3\sqrt6}$	$\dfrac{5}{9\sqrt6}$	$-\dfrac{7}{9\sqrt6}$
	$F'=9/2$	$-\dfrac{4}{9\sqrt3}$	$-\dfrac{2\sqrt7}{9\sqrt3}$	$-\dfrac{2}{3\sqrt3}$	$-\dfrac{2\sqrt{10}}{9\sqrt3}$	$-\dfrac{2\sqrt{10}}{9\sqrt3}$	$-\dfrac{2}{3\sqrt3}$	$-\dfrac{2\sqrt7}{9\sqrt3}$	$-\dfrac{4}{9\sqrt3}$
σ^-	$F'=7/2$	0	$\dfrac{7}{9\sqrt3}$	$\dfrac{2}{9}$	$\dfrac{\sqrt5}{9}$	$\dfrac{4}{9\sqrt3}$	$\dfrac{\sqrt5}{\sqrt6}$	$\dfrac{2}{9}$	$\dfrac{\sqrt7}{9\sqrt3}$
	$F'=9/2$	$-\dfrac{2\sqrt2}{3\sqrt3}$	$\dfrac{2\sqrt{14}}{9\sqrt3}$	$\dfrac{\sqrt{14}}{\sqrt9}$	$\dfrac{\sqrt{10}}{9}$	$\dfrac{2\sqrt5}{9\sqrt3}$	$\dfrac{2}{9}$	$\dfrac{\sqrt2}{9}$	$\dfrac{2}{9\sqrt3}$

Table 4: Coefficients $C_F(F, m_F, J, q)$ for hyperfine dipole matrix elements for EM transitions to the D1 ($^2\mathrm{P}_{1/2}$) manifold for $|F = ^7/_2, m_F\rangle \to |F', m'_F\rangle$, where $m'_F = m_F + 1$ for σ^+, $m'_F = m_F$ for π, and $m'_F = m_F - 1$ for σ^-.

m_F		$-9/2$	$-7/2$	$-5/2$	$-3/2$	$-1/2$	$1/2$	$3/2$	$5/2$	$7/2$	$9/2$
σ^+	$F' = {}^7/_2$	$\dfrac{2\sqrt{2}}{3\sqrt{3}}$	$\dfrac{2\sqrt{14}}{9\sqrt{3}}$	$\dfrac{\sqrt{14}}{9}$	$\dfrac{\sqrt{10}}{9}$	$\dfrac{2\sqrt{5}}{9\sqrt{3}}$	$\dfrac{2}{9}$	$\dfrac{\sqrt{2}}{9}$	$-\dfrac{\sqrt{2}}{9\sqrt{3}}$	0	0
	$F' = {}^9/_2$	$\dfrac{1}{3\sqrt{3}}$	$\dfrac{4}{9\sqrt{3}}$	$\dfrac{\sqrt{7}}{9}$	$\dfrac{2\sqrt{2}}{9}$	$\dfrac{5}{9\sqrt{3}}$	$\dfrac{2\sqrt{2}}{9}$	$\dfrac{\sqrt{7}}{9}$	$\dfrac{4}{9\sqrt{3}}$	$\dfrac{1}{3\sqrt{3}}$	0
π	$F' = {}^7/_2$	0	$\dfrac{4}{9\sqrt{3}}$	$\dfrac{2\sqrt{7}}{9\sqrt{3}}$	$\dfrac{2}{3\sqrt{3}}$	$\dfrac{4\sqrt{5}}{9\sqrt{6}}$	$\dfrac{4\sqrt{5}}{9\sqrt{6}}$	$\dfrac{2}{3\sqrt{3}}$	$\dfrac{2\sqrt{7}}{9\sqrt{3}}$	$\dfrac{4}{9\sqrt{3}}$	0
	$F' = {}^9/_2$	$-\dfrac{1}{\sqrt{6}}$	$-\dfrac{7}{9\sqrt{6}}$	$-\dfrac{5}{9\sqrt{6}}$	$-\dfrac{1}{3\sqrt{6}}$	$-\dfrac{1}{9\sqrt{6}}$	$\dfrac{1}{9\sqrt{6}}$	$\dfrac{1}{3\sqrt{6}}$	$\dfrac{5}{9\sqrt{6}}$	$\dfrac{7}{9\sqrt{6}}$	$\dfrac{1}{\sqrt{6}}$
σ^-	$F' = {}^7/_2$	0	0	$\dfrac{2}{9\sqrt{3}}$	$\dfrac{\sqrt{2}}{9}$	$\dfrac{2}{9}$	$\dfrac{2\sqrt{5}}{9\sqrt{3}}$	$\dfrac{\sqrt{10}}{9}$	$\dfrac{\sqrt{14}}{9}$	$\dfrac{4\sqrt{14}}{9\sqrt{3}}$	$\dfrac{2\sqrt{2}}{3\sqrt{3}}$
	$F' = {}^9/_2$	0	$-\dfrac{1}{3\sqrt{3}}$	$-\dfrac{4}{9\sqrt{3}}$	$-\dfrac{\sqrt{7}}{9}$	$-\dfrac{2\sqrt{2}}{9}$	$-\dfrac{5}{9\sqrt{3}}$	$-\dfrac{2\sqrt{2}}{9}$	$\dfrac{\sqrt{7}}{9}$	$-\dfrac{4}{9\sqrt{3}}$	$-\dfrac{1}{3\sqrt{3}}$

Table 5: Coefficients $C_F(F, m_F, J, q)$ for hyperfine dipole matrix elements for EM transitions to the D1 ($^2\mathrm{P}_{1/2}$) manifold for $|F = {}^9/_2, m_F\rangle \rightarrow |F', m'_F\rangle$, where $m'_F = m_F + 1$ for σ^+, $m'_F = m_F$ for π, and $m'_F = m_F - 1$ for σ^-.

m_F	$-7/2$	$-5/2$	$-3/2$	$-1/2$	$1/2$	$3/2$	$5/2$	$7/2$
σ^+ $F'=5/2$	$-\dfrac{\sqrt{3}}{4}$	$-\dfrac{\sqrt{15}}{4\sqrt{7}}$	$-\dfrac{\sqrt{5}}{2\sqrt{14}}$	$-\dfrac{\sqrt{3}}{2\sqrt{14}}$	$-\dfrac{\sqrt{3}}{4\sqrt{7}}$	$-\dfrac{1}{4\sqrt{7}}$	0	0
$F'=7/2$	$-\dfrac{\sqrt{10}}{9\sqrt{3}}$	$-\dfrac{2\sqrt{10}}{9\sqrt{7}}$	$-\dfrac{5\sqrt{2}}{9\sqrt{7}}$	$-\dfrac{4\sqrt{10}}{9\sqrt{21}}$	$-\dfrac{5\sqrt{2}}{9\sqrt{7}}$	$-\dfrac{2\sqrt{10}}{9\sqrt{7}}$	$-\dfrac{\sqrt{10}}{9\sqrt{3}}$	0
$F'=9/2$	$\dfrac{\sqrt{11}}{3\sqrt{36}}$	$\dfrac{\sqrt{11}}{36}$	$-\dfrac{\sqrt{11}}{18\sqrt{2}}$	$\dfrac{\sqrt{55}}{18\sqrt{6}}$	$\dfrac{\sqrt{55}}{36}$	$-\dfrac{\sqrt{77}}{36}$	$\dfrac{\sqrt{77}}{18\sqrt{3}}$	$\dfrac{\sqrt{11}}{6\sqrt{3}}$
π $F'=5/2$	0	$-\dfrac{\sqrt{3}}{2\sqrt{14}}$	$-\dfrac{\sqrt{5}}{2\sqrt{14}}$	$-\dfrac{\sqrt{3}}{2\sqrt{7}}$	$-\dfrac{\sqrt{3}}{2\sqrt{7}}$	$-\dfrac{\sqrt{5}}{2\sqrt{14}}$	$-\dfrac{\sqrt{3}}{2\sqrt{14}}$	0
$F'=7/2$	$\dfrac{\sqrt{35}}{9\sqrt{3}}$	$\dfrac{5\sqrt{5}}{9\sqrt{21}}$	$\dfrac{\sqrt{5}}{3\sqrt{21}}$	$\dfrac{\sqrt{5}}{9\sqrt{21}}$	$-\dfrac{\sqrt{5}}{9\sqrt{21}}$	$-\dfrac{\sqrt{5}}{3\sqrt{21}}$	$-\dfrac{5\sqrt{5}}{9\sqrt{21}}$	$-\dfrac{\sqrt{35}}{9\sqrt{3}}$
$F'=11/2$	$-\dfrac{\sqrt{11}}{9\sqrt{6}}$	$-\dfrac{\sqrt{77}}{18\sqrt{6}}$	$-\dfrac{\sqrt{11}}{6\sqrt{6}}$	$-\dfrac{\sqrt{55}}{18\sqrt{3}}$	$-\dfrac{\sqrt{55}}{18\sqrt{3}}$	$-\dfrac{\sqrt{11}}{6\sqrt{6}}$	$-\dfrac{\sqrt{77}}{18\sqrt{6}}$	$-\dfrac{\sqrt{11}}{9\sqrt{6}}$
σ^- $F'=7/2$	0	0	$-\dfrac{1}{4\sqrt{7}}$	$-\dfrac{\sqrt{3}}{4\sqrt{7}}$	$-\dfrac{\sqrt{3}}{2\sqrt{14}}$	$-\dfrac{\sqrt{5}}{2\sqrt{14}}$	$-\dfrac{\sqrt{15}}{4\sqrt{7}}$	$-\dfrac{\sqrt{3}}{4}$
$F'=9/2$	0	$\dfrac{\sqrt{10}}{9\sqrt{3}}$	$\dfrac{2\sqrt{10}}{9\sqrt{7}}$	$\dfrac{5\sqrt{2}}{9\sqrt{7}}$	$\dfrac{4\sqrt{10}}{9\sqrt{21}}$	$\dfrac{5\sqrt{2}}{9\sqrt{7}}$	$\dfrac{2\sqrt{10}}{9\sqrt{7}}$	$-\dfrac{\sqrt{10}}{9\sqrt{3}}$
$F'=11/2$	$\dfrac{\sqrt{11}}{6\sqrt{3}}$	$\dfrac{\sqrt{77}}{18\sqrt{3}}$	$\dfrac{\sqrt{77}}{36}$	$\dfrac{\sqrt{55}}{36}$	$\dfrac{\sqrt{55}}{18\sqrt{6}}$	$\dfrac{\sqrt{11}}{18\sqrt{2}}$	$\dfrac{\sqrt{11}}{36}$	$-\dfrac{\sqrt{11}}{36\sqrt{3}}$

Table 6: Coefficients $C_F(F, m_F, J, q)$ for hyperfine dipole matrix elements for EM transitions to the D2 ($^2\mathrm{P}_{3/2}$) manifold for $|F = {}^7/_2, m_F\rangle \rightarrow |F', m_F'\rangle$, where $m_F' = m_F + 1$ for σ^+, $m_F' = m_F$ for π, and $m_F' = m_F - 1$ for σ^-.

	m_F	$-9/2$	$-7/2$	$-5/2$	$-3/2$	$-1/2$	$1/2$	$3/2$	$5/2$	$7/2$	$9/2$
σ^+	$F'=7/2$	$-\dfrac{\sqrt7}{3\sqrt{15}}$	$-\dfrac{7}{9\sqrt{15}}$	$-\dfrac{7}{18\sqrt5}$	$-\dfrac{\sqrt7}{18}$	$-\dfrac{\sqrt7}{9\sqrt6}$	$-\dfrac{\sqrt7}{9\sqrt{10}}$	$-\dfrac{\sqrt7}{18\sqrt5}$	$-\dfrac{\sqrt7}{18\sqrt{15}}$	0	0
	$F'=9/2$	$-\dfrac{2\sqrt2}{3\sqrt{33}}$	$-\dfrac{8\sqrt2}{9\sqrt{33}}$	$-\dfrac{2\sqrt{14}}{9\sqrt{11}}$	$-\dfrac{8}{9\sqrt{11}}$	$-\dfrac{10\sqrt2}{9\sqrt{33}}$	$-\dfrac{8}{9\sqrt{11}}$	$-\dfrac{2\sqrt{14}}{9\sqrt{11}}$	$-\dfrac{8\sqrt2}{9\sqrt{33}}$	$-\dfrac{2\sqrt2}{3\sqrt{33}}$	0
	$F'=11/2$	$-\dfrac{1}{2\sqrt{55}}$	$-\dfrac{\sqrt3}{2\sqrt{55}}$	$-\dfrac{\sqrt3}{\sqrt{110}}$	$-\dfrac{1}{\sqrt{22}}$	$-\dfrac{\sqrt3}{2\sqrt{11}}$	$-\dfrac{\sqrt{21}}{2\sqrt{55}}$	$-\dfrac{\sqrt7}{\sqrt{55}}$	$-\dfrac{3}{\sqrt{55}}$	$-\dfrac{3}{2\sqrt{11}}$	$\dfrac12$
π	$F'=7/2$	0	$-\dfrac{\sqrt{14}}{9\sqrt{15}}$	$-\dfrac{7}{9\sqrt{30}}$	$-\dfrac{\sqrt7}{3\sqrt{30}}$	$-\dfrac{\sqrt7}{9\sqrt3}$	$-\dfrac{\sqrt7}{9\sqrt3}$	$-\dfrac{\sqrt7}{3\sqrt{30}}$	$-\dfrac{7}{9\sqrt{30}}$	$-\dfrac{\sqrt{14}}{9\sqrt{15}}$	0
	$F'=9/2$	$\dfrac{2}{\sqrt{33}}$	$\dfrac{14}{9\sqrt{33}}$	$\dfrac{10}{9\sqrt{33}}$	$\dfrac{2}{3\sqrt{33}}$	$\dfrac{2}{9\sqrt{33}}$	$-\dfrac{2}{9\sqrt{33}}$	$-\dfrac{2}{3\sqrt{33}}$	$-\dfrac{10}{9\sqrt{33}}$	$-\dfrac{14}{9\sqrt{33}}$	$-\dfrac{2}{\sqrt{33}}$
	$F'=11/2$	$-\dfrac{1}{\sqrt{22}}$	$-\dfrac{3}{3\sqrt{110}}$	$-\dfrac{\sqrt6}{\sqrt{55}}$	$-\dfrac{\sqrt7}{\sqrt{55}}$	$-\dfrac{\sqrt3}{\sqrt{22}}$	$-\dfrac{\sqrt3}{\sqrt{22}}$	$-\dfrac{\sqrt7}{\sqrt{55}}$	$-\dfrac{\sqrt6}{\sqrt{55}}$	$-\dfrac{3}{3\sqrt{110}}$	$-\dfrac{1}{\sqrt{22}}$
σ^-	$F'=7/2$	0	0	$-\dfrac{\sqrt7}{18\sqrt{15}}$	$-\dfrac{\sqrt7}{18\sqrt5}$	$-\dfrac{\sqrt7}{9\sqrt{10}}$	$-\dfrac{\sqrt7}{9\sqrt6}$	$-\dfrac{\sqrt7}{18}$	$-\dfrac{7}{18\sqrt5}$	$-\dfrac{7}{9\sqrt{15}}$	$-\dfrac{\sqrt7}{3\sqrt{15}}$
	$F'=9/2$	0	$-\dfrac{2\sqrt2}{3\sqrt{33}}$	$-\dfrac{8\sqrt2}{9\sqrt{33}}$	$-\dfrac{2\sqrt{14}}{9\sqrt{11}}$	$-\dfrac{8}{9\sqrt{11}}$	$-\dfrac{10\sqrt2}{9\sqrt{33}}$	$-\dfrac{8}{9\sqrt{11}}$	$-\dfrac{2\sqrt{14}}{9\sqrt{11}}$	$-\dfrac{8\sqrt2}{9\sqrt{33}}$	$-\dfrac{2\sqrt2}{3\sqrt{33}}$
	$F'=11/2$	$\dfrac12$	$-\dfrac{3}{2\sqrt{11}}$	$-\dfrac{3}{\sqrt{55}}$	$-\dfrac{\sqrt7}{\sqrt{55}}$	$-\dfrac{\sqrt{21}}{2\sqrt{55}}$	$-\dfrac{\sqrt3}{2\sqrt{11}}$	$-\dfrac{1}{\sqrt{22}}$	$-\dfrac{\sqrt3}{\sqrt{110}}$	$-\dfrac{\sqrt3}{2\sqrt{55}}$	$-\dfrac{1}{2\sqrt{55}}$

Table 7: Coefficients $C_F(F, m_F, J, q)$ for hyperfine dipole matrix elements for EM transitions to the D2 ($^2\mathrm{P}_{3/2}$) manifold for $|F = {}^9\!/_2, m_F\rangle \rightarrow |F', m'_F\rangle$, where $m'_F = m_F + 1$ for σ^+, $m'_F = m_F$ for π, and $m'_F = m_F - 1$ for σ^-.

6 A few practicalities

The above calculations are more than just an academic exercise. The values found are useful in the design and implementation of experiments involving ^{40}K. In the following, I describe two examples of how this information will be of use in the laboratory.

Many fermion experiments are working towards the realisation of superfluidity in a dilute atomic gas [25]. To do this, the scattering length between particles (and the corresponding interaction potential) must be made large such that the transition temperature to the superfluid state is high enough to be experimentally observable [26].In general, this is accomplished through a Feshbach resonance [27] - the magnetic field is tuned to a value where a bound state for the molecular dimer is of the same energy as the free particles. This resonance creates the strong interaction between particles. As such, working in strong magnetic fields is necessary.

It may be interesting to consider the transition matrix elements between states in the intermediate field, where neither the $|F, m_F\rangle$ nor the $|J, m_J, I, m_I\rangle$ are good eigenstates. By using the results of the numerical diagonalisation, we can write down the state at a given magnetic field as linear combination of $|J, m_J, I, m_I\rangle$ states. To give an example, let us consider the transition from the ground state connected to $|F = {}^9/_2, m_F = {}^5/_2\rangle$ and $|m_J = {}^{-1}/_2, m_I = 3\rangle$ and to the D2 excited state connected to $|F = {}^5/_2, m_F = {}^5/_2\rangle$ and $|m_J = {}^3/_2, m_I = 1\rangle$ at a magnetic field of 85 gauss. Note that this transition is forbidden in the zero-field limit ($\Delta m_F = 2$) and in the high field limit ($\Delta m_I \neq 0$). In the $|m_J, m_I\rangle$ basis, the eigenstates for the ground and excited states are, respectively:

$$|\psi_{\text{ground}}\rangle = -0.5473| - {}^1/_2, 3\rangle + 0.8370|{}^1/_2, 2\rangle \tag{46}$$

$$|\psi_{\text{D2}}\rangle = -0.0003| - {}^3/_2, 4\rangle + 0.0127| - {}^1/_2, 3\rangle - 0.1690|{}^1/_2, 2\rangle + 0.9855|{}^3/_2, 1\rangle. \tag{47}$$

To determine the appropriate transition matrix element, we consider

$$
\begin{aligned}
\langle \psi_{\text{ground}}|\mathbf{d}|\psi_{\text{D2}}\rangle &= -0.0070\langle {}^{-1}/_2, 3|\mathbf{d}| {}^{-1}/_2, 3\rangle - 0.1415\langle {}^1/_2, 2|\mathbf{d}|{}^1/_2, 2\rangle \\
&= \langle {}^1/_2||\mathbf{d}||{}^3/_2\rangle \left[0.0070 \begin{pmatrix} {}^1/_2 & 1 & {}^3/_2 \\ {}^1/_2 & \text{q} & {}^{-1}/_2 \end{pmatrix} \right. \\
&\qquad \left. -0.1415 \begin{pmatrix} {}^1/_2 & 1 & {}^3/_2 \\ -{}^1/_2 & \text{q} & {}^1/_2 \end{pmatrix} \right] \\
&= -0.055\langle {}^1/_2||\mathbf{d}||{}^3/_2\rangle \qquad \text{ifq} = 0 \tag{48}
\end{aligned}
$$

where terms that are disallowed by the selection rule $\Delta m_I = 0$ have been omitted. We see that, for π light ($q = 0$) there is some probability for the transition in the presence of a magnetic field, even though it is forbidden in both high and low fields. It is important to consider which transitions are possible at each field if accurate imaging is to be performed, as one could imagine exciting unexpected transitions, realising more absorption than accounted for, and miscalculating such things as atom numbers. The apparent selection rule
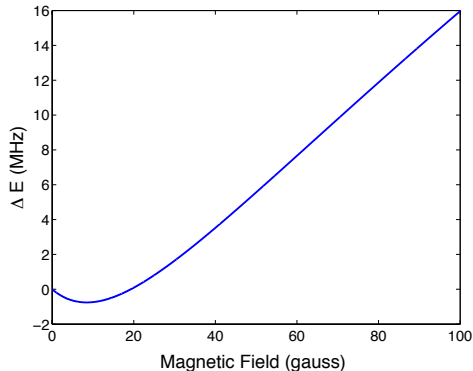
Figure 5: Difference in resonance condition for two hyperfine transitions. This difference in energy, ΔE, is defined as the energy for the σ^+ transition from the $|F = 9/2, m_F = 7/2\rangle$ less the $|F = 9/2, m_F = 9/2\rangle$ states. (Note that the validity of these eigenstates begins to fail at higher magnetic fields)

that remains firm is that $m_F - m'_F = \pm 1$ or 0, though we may now violate the rules for F and m_I.

In addition, the application of a magnetic field makes the energies of different hyperfine states dependent on the magnetic field. To realise the superfluid regime, non-identical particles must interact. This non-identicality is generally realised by using two spin states of the same atom in ^{40}K, the $|F = 9/2, m_F = 9/2\rangle$ and $|F = 9/2, m_F = 7/2\rangle$ [28]. Looking at Figs. (2), (4), we see that the energy of the transition from ground to excited state is dependent on magnetic field. If we wish to image only one spin state, we could choose a magnetic field at which the resonance condition is significantly different (i.e. greater than a linewidth) from the other.

In these experiments, data is generally collected via absorption imaging. The principle of this technique is that light resonant to a transition between hyperfine states is absorbed by the atoms. The amount of light absorbed is recorded, and from this, one can determine such things as temperature and momentum distributions. Assuming we image with σ^+ light, which as seen in Table 7 has a high transition probability, then we can plot the energy of the transition as a function of magnetic field by simply subtracting the two appropriate curves in Figs. (2), (4). Figure 5 shows this result. We find here that a magnetic field of ≈ 80 gauss is required to separate the energy levels by a linewidth ($1/tau_{life} = 2\pi$ 5.9 MHz). This separation allows the distinction between different states to be done on the basis of the frequency of light.

7 Conclusion

Despite its small natural abundance, ^{40}K has risen to special status due to its being one of the two stable fermionic isotopes among the alkalis. Experiments using ultra-cold, quantum degenerate fermions have been used to demonstrate a number of fundamental physical phenomena, including superfluidity, and have the promise of delivering insight into unknown physical problems [29]. Precise control over the internal states of the atoms in these experiments is necessary for the realisation of these experiments. A good knowledge of the hyperfine structure of the two strongest transitions, the D1 and D2 lines, allows for this manipulation.

This report outlined the origin of the hyperfine splitting, looking at effects from both the nuclear spin and the quadrupole moment. The hyperfine splitting has been calculated in all regimes of magnetic field. A derivation of the transition matrix elements between states under the influence of optical radiation has been given, and the results of these for all transitions between ground and D1 and D2 excited states have been tabulated. Finally, two applications of these results are given as apply to experiments currently being performed.

Appendix A: Useful matrix elements

Some of the useful matrix elements for calculating the appropriate matrix elements of the Hamiltonian (32) can be determined using Eq. (33) and are stated as follows:

$$
\begin{aligned}
\langle J, m_J, I, m_I | \mathbf{I} \cdot \mathbf{J} | J, m_J, I, m_I \rangle &= m_J m_I \\
\langle J, m_J, I, m_I | \mathbf{I} \cdot \mathbf{J} | J, m_J + 1, I, m_I - 1 \rangle &= \frac{1}{2} \sqrt{(J + m_J)(J - m_J + 1)} \\
&\quad \times \sqrt{(I - m_I)(I + m_I + 1)} \\
\langle J, m_J, I, m_I | \mathbf{I} \cdot \mathbf{J} | J, m_J - 1, I, m_I + 1 \rangle &= \frac{1}{2} \sqrt{(J - m_J)(J + m_J + 1)} \\
&\quad \times \sqrt{(I + m_I)(I - m_I + 1)}
\end{aligned}
$$

$$(49)$$

Similarly, for the electric quadrupole term, expressions for the matrix elements of the operator (35) can be determined and are found in Appendix C of

Ref. [14]:

$$\langle m_J, m_I|f|m_J, m_I\rangle = \frac{1}{2}\left[\frac{3}{2}m_I^2 - I(I+1)\right]\left[3m_J^2 - J(J+1)\right]$$

$$\langle m_J, m_I|f|m_J - 1, m_I + 1\rangle = \frac{3}{4}(2m_J - 1)(2m_I + 1)$$
$$\times\left[(J + m_J)(J - m_J + 1)(I - m_I)(I + m_I + 1)\right]^{\frac{1}{2}}$$

$$\langle m_J, m_I|f|m_J + 1, m_I - 1\rangle = \frac{3}{4}(2m_J + 1)(2m_I - 1)$$
$$\times\left[(J - m_J)(J + m_J + 1)(I + m_I)(I - m_I + 1)\right]^{\frac{1}{2}}$$

$$\langle m_J, m_I|f|m_J - 2, m_I + 2\rangle = \frac{3}{4}\big[(J + m_J)(J + m_J + 1)(J - m_J + 1)(J - m_J + 2)$$
$$\times(I - m_I)(I - m_I - 1)(I + m_I + 1)(I + m_I + 2)\big]^{\frac{1}{2}}$$

$$\langle m_J, m_I|f|m_J + 2, m_I - 2\rangle = \frac{3}{4}\big[(J - m_J)(J - m_J - 1)(J + m_J + 1)(J + m_J + 2)$$
$$\times(I + m_I)(I + m_I - 1)(I - m_I + 1)(I - m_I + 2)\big]^{\frac{1}{2}}$$

$$(50)$$

References

[1] H. Anderson, J.R. Ensher, M.R. Matthews, C.E. Wieman, and E. A. Cornell, *Science* **269** 198 (1995); K.B. Davis, M.-O. Mewes, M.R. Andrews, N.J. van Druten, D.S. Durfee, D.M. Kurn, and W. Ketterle, *Phys. Rev. Lett.* **75**, 3969 (1995); C. C. Bradley, C.A. Sackett, J.J. Tollett, and R. G. Hulet, *Phys. Rev. Lett.* **75**, 1687 (1995); see also C.A. Sackett, C.C. Bradley, M. Welling, and R.G. Hulet, *Appl. Phys. B* **B65**, 433 (1997)..

[2] A. Peters, K.Y. Chung and S. Chu, *Nature*, **400**, 849 (1999).

[3] M. Greiner, O. Mandel, T. Esslinger, T.W. Hänsch and I. Bloch, *Nature*, **415**, 39 (2002).

[5] K.B. Davis, M.-O. Mewes, and W. Ketterle, *Appl. Phys. B.* **60**, 155 (1995).

[6] B. DeMarco and D. S. Jin, *Science* **285**, 1703 (1999); A. G. Truscott, K. E. Strecker, W. I. McAlexander, G. B. Partridge, and R. G. Hulet, *Science* **291**, 2570 (2001); F. Schreck, L. Khaykovich, K. L. Corwin, G. Ferrari, T. Bourdel, J. Cubizolles, and C. Salomon, *Phys. Rev. Lett.* **87**, 080403 (2001); S. R. Granade, M. E. Gehm, K. M. O'Hara, and J. E. Thomas, *Phys. Rev. Lett.* **88**, 120405 (2002); G. Roati, F. Riboli, G. Modugno, and M. Inguscio, Phys. Rev. Lett. **89**, 150403 (2002).

[7] D.A. Steck. Rubidium 87 D Line Data, rev. 1.6. available at: http://george.ph. utexas.edu/ dsteck/alkalidata/rubidium87numbers.pdf (14 October 2003).

[8] J.J. Sakurai. Modern Quantum Mechanics. (Addison-Wesley: 1994).

[9] Potassium: NMR Data. WebElements Periodic Table. http://www.webelements.com /webelements/elements/text/K/nucl.html (11 April 2006).

[10] NIST Atomic Spectra Database Levels Data: K I. http://physics.nist.gov/ PhysRefData/ASD/levels_form.html (11 April 2006).

[12] G.K. Woodgate. Elementary Atomic Structure, 3rd ed. (Clarendon Press: 1980) Ch. 9.

[13] C. Cohen-Tannoudji, B. Diu, F. Laloë. Quantum Mechanics. (John Wiley and Sons: 1977), Ch. XII.

[14] N.F. Ramsey. Molecular Beams. (Oxford University Press: 1956).

[15] N.F. Ramsey. Nuclear Moments. (John Wiley and Sons: 1953).

[16] F. Touchard *et. al. Phys. Lett.* **108**, 169 (1982).

[17] N. Bendali, H.T. Duong, & J.L. Vialle. *J. Phys. B. At. Mol. Phys.* **14**, 4231 (1981).

[18] E. Arimondo, M. Inguscio, P. Violino. Experimental determinations of the hyperfine structure in the alkali atoms. *Rev. Mod. Phys.* **49**, 31 (1977).

[19] NIST Reference on Constants, Units and Uncertainty (CODATA Internationally recommended values of the fundamental physical constants (2002)), available at http://physics.nist.gov/cuu/Constants/.

[20] Lectures in PHY 2206S, Atomic, Molecular and Optical Physics, D.F.V. James, University of Toronto (January - April 2006).

[21] R. Loudon. The Quantum Theory of Light, 3rd ed. (Oxford University Press: 2000), p 52.

[22] U. Volz & H. Schmoranzer. *Physica Scripta* **T65**, 48 (1996).

[23] L. Bergmann & C. Schaeffer. Constituents of Matter: Atoms, Molecules, Nuclei and Particles. (Walter de Gruyter: 1997) §1.7.3.1.

[24] L.D. Landau & E.M. Lifshitz. Quantum Mechanics: Non-relativistic theory, 3rd ed. (Pergamon Press: 1976) §109.

[25] C. A. Regal, M. Greiner, and D. S. Jin, *Phys. Rev. Lett.*, **92**, 040403 (2004); M. Bartenstein, A. Altmeyer, S. Riedl, S. Jochim, C. Chin, J. Hecker Denschlag, and R. Grimm, *Phys. Rev. Lett.*, **92**, 120401 (2004); T. Bourdel, L. Khaykovich, J. Cubizolles, J. Zhang, F. Chevy, M. Teichmann, L. Tarruell, S. J. J. M. F. Kokkelmans, C. Salomon, *Phys. Rev. Lett.*, **93**, 050401 (2004); M. W. Zwierlein, C. A. Stan, C. H. Schunck, S. M. F. Raupach, A. J. Kerman, W. Ketterle, *Phys. Rev. Lett.*, **92**, 120403 (2004).

[26] P. Nozires and S. Schmidt-Rink. Bose Condensation in an Attractive Fermion Gas. *J. Low Temp. Phys.*, **59**, 195 (1985).

[27] A. Simoni, F. Ferlaino, G. Roati, G. Modugno, M. Inguscio. Magnetic control of the interacction in ultracold K-Rb mixtures. *Phys. Rev. Lett.* **90**, 163202 (2003); C. Ticknor, C.A. Regal, D.S. Jin, & J.L. Bohn. Multiplet structure of Feshbach resonances in nonzero partial waves. *Phys. Rev. A* **69**, 042712 (2004).

[28] C. A. Regal, M. Greiner, and D. S. Jin, *Phys. Rev. Lett.*, **92**, 040403 (2004).

[29] W. Hofstetter, J. I. Cirac, P. Zoller, E. Demler, and M. D. Lukin, *Phys. Rev. Lett.*, **89**, 220407 (2002).